

PAPER: CLASSICAL STATISTICAL MECHANICS, EQUILIBRIUM AND NON-EQUILIBRIUM

## Percolation in irreversible deposition on a triangular lattice: effects of anisotropy

To cite this article: I Lonarevi *et al* *J. Stat. Mech.* (2020) 033211

View the [article online](#) for updates and enhancements.



**IOP | ebooks™**

Bringing you innovative digital publishing with leading voices  
to create your essential collection of books in STEM research.

Start exploring the **collection** - **download the first chapter of  
every title for free.**

# Percolation in irreversible deposition on a triangular lattice: effects of anisotropy

I Lončarević<sup>1</sup>, Lj Budinski-Petković<sup>1</sup>, D Dujak<sup>2</sup>, A Karač<sup>3</sup>,  
Z M Jakšić<sup>3</sup> and S B Vrhovac<sup>4</sup>

<sup>1</sup> Faculty of Engineering, Trg D. Obradovića 6, Novi Sad 21000, Serbia

<sup>2</sup> Faculty of Electrical Engineering, University of Sarajevo, Zmaja od Bosne, University campus, 71000 Sarajevo, Bosnia and Herzegovina

<sup>3</sup> Polytechnic Faculty, University of Zenica, 72000 Zenica, Bosnia and Herzegovina

<sup>4</sup> Institute of Physics, Belgrade, Pregrevica 118 Zemun 11080, Belgrade, Serbia  
E-mail: [ivanalon@uns.ac.rs](mailto:ivanalon@uns.ac.rs)

Received 19 November 2019

Accepted for publication 3 February 2020

Published 18 March 2020



Online at [stacks.iop.org/JSTAT/2020/033211](https://stacks.iop.org/JSTAT/2020/033211)  
<https://doi.org/10.1088/1742-5468/ab780a>

**Abstract.** The percolation properties in anisotropic irreversible deposition of extended objects are studied by Monte Carlo simulations on a triangular lattice. Depositing objects of various shapes and sizes are made by directed self-avoiding walks on the lattice. Anisotropy is introduced by imposing unequal probabilities for placing the objects along different directions of the lattice. The degree of the anisotropy is characterized by the order parameter  $p$  determining the probability for deposition in the chosen (horizontal) direction. For each of the other two directions adsorption occurs with probability  $(1 - p)/2$ . It is found that the percolation threshold  $\theta_p$  increases with the degree of anisotropy, having the maximum values for fully oriented objects. Percolation properties of the elongated shapes, such as  $k$ -mers, are more affected by the presence of anisotropy than the compact ones.

Percolation in anisotropic deposition was also studied for a lattice with point-like defects. For elongated shapes a slight decrease of the percolation threshold with the impurity concentration  $d$  can be observed. However, for these shapes,  $\theta_p$  significantly increases with the degree of anisotropy. In the case when depositing objects are triangles, results are qualitatively different.

The percolation threshold decreases with  $d$ , but is not affected by the presence of anisotropy.

**Keywords:** numerical simulations, percolation problems

---

## Contents

|                                                                                      |           |
|--------------------------------------------------------------------------------------|-----------|
| <b>1. Introduction</b>                                                               | <b>2</b>  |
| <b>2. Definition of the model and the simulation method</b>                          | <b>4</b>  |
| <b>3. Results and discussion</b>                                                     | <b>5</b>  |
| 3.1. Effects of anisotropy .....                                                     | 7         |
| 3.2. Percolation in anisotropic conditions on a lattice with point-like defects..... | 15        |
| <b>4. Concluding remarks</b>                                                         | <b>17</b> |
| <b>Acknowledgments</b> .....                                                         | <b>17</b> |
| <b>References</b>                                                                    | <b>18</b> |

---

## 1. Introduction

Irreversible adsorption has a wide range of applications in biology, nanotechnology, material science, and device physics [1–3]. Depending on the system of interest, depositing objects can be various macromolecules, proteins, DNA segments, polymer chains, nanotubes, etc. There is a large number of works dealing with deposition of regular shapes on spatially homogeneous regular surfaces, but recent interest has shifted to deposition of irregular shapes on patterned or inhomogeneous substrates [4–7]. In real physical situations substrates can be biological membranes, minerals, and other inherently heterogeneous surfaces. Understanding the impact of surface topography is crucial for controlling the adsorption process.

Irreversible deposition is often studied by random sequential adsorption model (RSA). In these models particles are randomly, sequentially and irreversibly deposited onto a substrate. The particles are not allowed to overlap, so the dominant effect in RSA is the blocking of the available substrate area and the limiting (jamming)  $\theta_{\text{jam}}$  coverage is less than in close packing. The kinetic properties of a deposition process are described by the time evolution of the coverage  $\theta(t)$ , that is the fraction of the substrate area occupied by the adsorbed particles [8–10]. Since the process of object deposition is random, the quantity  $\theta(t)$  represents the expected value of the coverage at time  $t$ .

Depending on the system of interest, the substrate can be continuum or discrete, and RSA models can differ in substrate dimensionality. Exact solutions are available only for a number of one-dimensional problems [11, 12]. Due to the complexity of the geometrical exclusion effects in two and three dimensions, Monte Carlo simulations are one of the primary investigating tools for these deposition processes [13–18].

The long-term behavior of the coverage fraction is known to be algebraic for continuum systems [1, 14], and exponential for lattice models [15, 17]. For discrete substrates the late time kinetics of the process is described by the time dependence:

$$\theta(t) = \theta_{\text{jam}} - Ae^{-t/\tau}, \quad (1)$$

where  $A$  and  $\tau$  are parameters that depend on the shape, orientational freedom of the objects, and on the substrate dimensionality and heterogeneity.

During the process of irreversible deposition, coverage increases causing the growth of clusters of occupied sites. Percolation assumes the formation of a large cluster that connects two opposite sides of the substrate [19]. The interplay between RSA and percolation has been discussed in several works [20–22]. Motivated by irreversible deposition of large particles, such as polymers, the percolation properties of flexible chains were discussed in [23] for both the square and the triangular lattice. Simulations were performed for various chain lengths and the compositions that give minimum percolation thresholds were identified. For longer and more bent chains non-percolation regime was observed. Results for the percolation thresholds, jamming coverages, and their ratios for deposition of various objects on a triangular lattice were presented in [24]. Depositing objects of various shapes were made by self-avoiding random walks on the lattice. It was found that the percolation threshold monotonically decreases for elongated shapes and increases for more compact objects with the object size. For compact objects of larger sizes jamming coverage was reached before the percolation.

In order to describe the inhomogeneous surfaces in the RSA model, anisotropy in the deposition procedure can be imposed [25]. Namely, the probability for deposition is different along different directions of the underlying lattice. This simple modification introduces preferential direction in the deposition process and causes a specific ‘patterning’ of the deposited layer. Effect of anisotropy on the RSA of objects of various shapes on a triangular lattice was studied by Monte Carlo simulations [26]. It was shown that the kinetics of anisotropic deposition strongly depends on the symmetry properties of the object. In the case of elongated and asymmetric shapes, the relaxation time was found to increase with the degree of anisotropy. However, for symmetric shapes, rapidity of the approach to the jamming state was not affected by the presence of anisotropy. For asymmetric shapes the jamming coverage was also found to depend on the degree of anisotropy.

Effect of anisotropy on the electrical conductivity in disordered systems, such as polymer chains and nanotubes, was studied experimentally in [27]. It was found that percolation conductivity of a stick network depends on the alignment, as well as on the concentration. The highest conductivity occurs for slightly aligned, rather than isotropic sticks. Electrical conductivity of a monolayer produced by random sequential adsorption of linear  $k$ -mers onto a square lattice was examined by computer simulations [28]. Isotropic deposition with two possible orientations of the  $k$ -mers along the  $x$  and  $y$  axes, and anisotropic deposition with all the  $k$ -mers oriented in the  $y$  direction were analyzed. Percolation phenomena were also investigated for anisotropic random sequential adsorption of  $k$ -mers on a square lattice by Monte Carlo simulations for various values of order parameter [29]. For partially ordered systems, for a certain length of  $k$ -mers, a minimum of the percolation threshold value has been observed. It has been

found that the increase of system ordering always results in an increase of the percolation threshold.

Percolation with the presence of impurities has also been studied [30, 31]. It has been shown that the critical defect concentration, i.e. the highest concentration for which the percolation was observed, depends on the object shape. Effect of anisotropy on jamming and percolation for RSA of linear  $k$ -mers on a square lattice that contains defects was studied in [32]. The critical concentration of defects was found to decrease with the order parameter determining the degree of anisotropy.

Here we investigate the percolation properties in irreversible deposition of objects of various shapes on inhomogeneous substrates. Most of the work is devoted to percolation in anisotropic conditions, with various probabilities for depositions in a certain direction, i.e. for various values of the order parameter. Effects of anisotropy is also studied for lattices with quenched impurities.

The paper is organized as follows. Section 2 describes the details of the model and simulations. Results and discussions are given in section 3, while section 4 contains some additional comments and final remarks.

## 2. Definition of the model and the simulation method









Anisotropic irreversible deposition of extended objects is studied by Monte Carlo simulations. The depositing objects are modeled by self-avoiding walks on a triangular lattice. A self-avoiding walk of length  $\ell$  is a sequence of distinct sites of the lattice such that each site is a nearest neighbor of its predecessor, so a walk of length  $\ell$  covers  $\ell + 1$  lattice sites.

Anisotropy is introduced by imposing different probabilities of deposition in the three possible directions. The choice of the horizontal direction occurs with probability  $p$  and for each of the other two directions with probability  $(1 - p)/2$ . Hence, the value of  $p = 1/3$  corresponds to the isotropic case. In our simulations one direction corresponds to two opposite orientations with equal deposition probabilities. The probability  $p$  actually stands for the order parameter characterizing the degree of anisotropy.









At each Monte Carlo step a lattice site is selected uniformly at random. If the selected site is unoccupied, one of the six possible orientations is chosen with the corresponding probability and deposition of the object is tried in that orientation. We fix the beginning of the walk that makes the shape at the selected site and search whether all successive  $\ell$  sites are unoccupied. If so, we occupy these  $\ell + 1$  sites and place the object. If the attempt fails, a new site is selected at random. The jamming limit is reached when the object of the specified shape cannot be placed in any position on the lattice.

In this work we concentrate on the study of percolation in anisotropic irreversible deposition. The coverage of the surface is increased in the RSA process up to the percolation threshold, when there appears a cluster that extends through the whole system—from the left to the right side of the lattice. The tree-based union/find algorithm is used to determine the percolation threshold [33]. Each cluster of connected sites is stored as a separate tree, having a single ‘root’ site. All sites of the cluster possess pointers to the root site, so it is simple to ascertain whether two sites are members of the same

**Table 1.** Various shapes ( $x$ ) of length  $\ell$  on a triangular lattice. Here  $n_s$  denotes the order of the symmetry axis of the shape.

| ( $x$ ) | Shape                                                                             | $\ell$ | $n_s$ |
|---------|-----------------------------------------------------------------------------------|--------|-------|
| (A)     |  | 1      | 2     |
| (B)     |  | 2      | 1     |
| (C)     |  | 2      | 3     |
| (D)     |  | 3      | 1     |
| (E)     |  | 3      | 2     |
| (F)     |  | 3      | 1     |
| (G)     |  | 3      | 1     |
| (H)     |  | 3      | 2     |

**Table 2.** Illustration of the construction of the objects larger than the basic ones.

| Shape                                                                               | $A\ell$     | Shape                                                                               | $B\ell$     | Shape                                                                               | $C\ell$     | Shape                                                                                 | $H\ell$     |
|-------------------------------------------------------------------------------------|-------------|-------------------------------------------------------------------------------------|-------------|-------------------------------------------------------------------------------------|-------------|---------------------------------------------------------------------------------------|-------------|
|    | $\ell = 1$  |    | $\ell = 2$  |    | $\ell = 2$  |    | $\ell = 3$  |
|  | $\ell = 2$  |  | $\ell = 3$  |  | $\ell = 5$  |  | $\ell = 8$  |
| ...                                                                                 | ...         | ...                                                                                 | ...         | ...                                                                                 | ...         | ...                                                                                   | ...         |
| ...                                                                                 | $\ell = 10$ | ...                                                                                 | $\ell = 20$ | ...                                                                                 | $\ell = 20$ | ...                                                                                   | $\ell = 24$ |

cluster. When a deposited object connects two separate clusters, they are amalgamated by adding a pointer from the root of the smaller cluster to the root of the larger one. This procedure is repeated until the percolation threshold is reached, i.e. until the opposite sites of the lattice are connected by a single cluster. The cluster wrapping making the percolation through the lattice can be defined in a number of different ways [29]. In the isotropic case the percolation thresholds have equal values along all directions. Nevertheless, for an anisotropic system we have to define the direction of interest for percolation. Here we determine the average coverage when a left–right crossing first appears. In the following text we denote this value as the percolation threshold  $\theta_p$ .

The Monte Carlo simulations are performed on a triangular lattice of size up to  $L = 3200$ . Periodic boundary conditions are used in all directions. The time is counted by the number of attempts to select a lattice site and scaled by the total number of lattice sites (discrete time model). In all the simulations the data are averaged over 500 independent runs.

### 3. Results and discussion

Jamming coverages and percolation thresholds are determined for a large variety of objects. Basic object shapes made by the self-avoiding walks of length  $\ell = 1, 2$ , and 3 are shown in table 1. Objects of larger sizes are made by repeating each step of a basic shape the same number of times for the elongated shapes, while the compact objects of larger sizes, such as triangles and rhombuses, also occupy all comprised sites. The

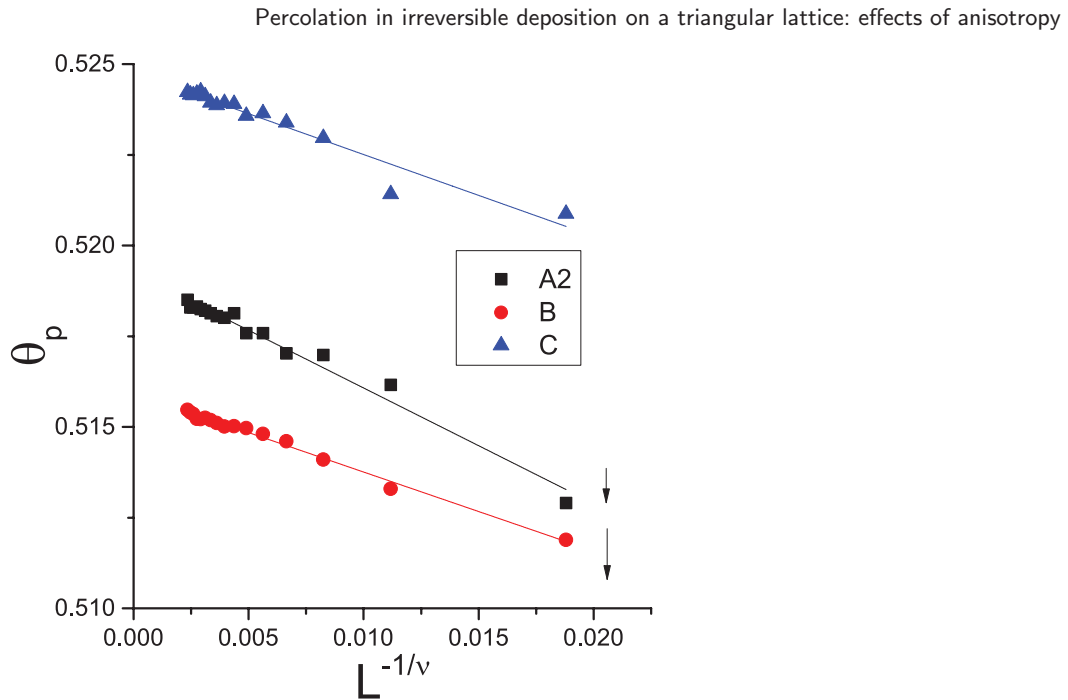


**Figure 1.** Finite-size scaling of the mean value of the percolation threshold  $\theta_p$  versus  $L^{-1/\nu}$  for objects (A2), (B), and (C) for the value of the order parameter  $p = 0.84$ . Straight lines represent the linear fit of the form:  $\theta_p - \theta_p^* \propto L^{-1/\nu}$ , where the asymptotic value of the percolation threshold  $\theta_p^*$  coincides with the value  $\theta_p$  obtained for the largest lattice, within the statistical error. For clarity, the data for objects (A2) and (B) are shifted vertically upward by 0.022 and 0.0415, respectively.

construction of larger objects is illustrated in table 2. Simulations are performed for  $k$ -mers (denoted as (A), angled objects (B), and triangles (C) up to the length  $\ell = 20$ , for objects (D), (E), (F), (G) up to  $\ell = 21$ , and for rhombuses less than  $\ell = 15$  because the percolation cannot be reached for larger ones.

According to the scaling theory the effective percolation threshold  $\theta_p$  (the mean value measured for a finite lattice) approaches the asymptotic value  $\theta_p^*$  ( $L \rightarrow \infty$ ) via the power law [19]:

$$\theta_p - \theta_p^* \propto L^{-1/\nu}. \quad (2)$$

For all lattice sizes and all examined objects results for the percolation thresholds are averaged over 500 independent runs. The theoretical value for the critical exponent is  $\nu = 4/3$  for two-dimensional systems. For the objects (A2), (B) and (C) simulations are performed for the lattice size ranging from  $L = 200$  to  $L = 3200$ . Plots of the mean value of  $\theta_p$  obtained for various lattice sizes against  $L^{-1/\nu}$  are shown in figure 1 in the case of anisotropic deposition  $p = 0.84$ . It must be stressed that validity of the finite-size scaling is confirmed in the whole range of parameter  $p$ . Moreover, the asymptotic value of the percolation threshold  $\theta_p^*$  coincides with the value of  $\theta_p$  obtained for the largest lattice, within the limits of the statistical error. Although  $\theta_p$  is sensitive to the lattice size  $L$ ,  $\theta_p$  tends to  $\theta_p^*$  as  $L \rightarrow \infty$ . As also confirmed in [23, 34], the results for a

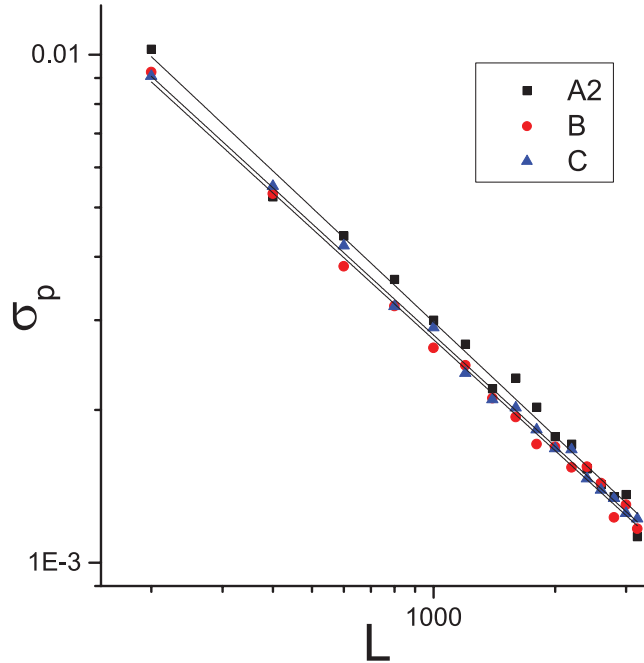


**Figure 2.** Finite-size scaling of the mean value of the standard deviation  $\sigma_p$  against  $L$  for objects (A2), (B), and (C) for the value of the order parameter  $p = 0.84$ . Straight lines represent the linear fit of the form:  $\sigma_p \propto L^{-1/\nu}$ .

sufficiently large lattice can be taken instead of the asymptotic value  $\theta_p^*$ . For further analysis of the percolation threshold we take the results for  $L = 3200$ .

According to the scaling theory [19] the standard deviation  $\sigma_p$  of the percolation threshold determined for a finite size lattice  $L$  satisfies the power law:

$$\sigma_p \propto L^{-1/\nu}. \quad (3)$$

In the case under consideration,  $\sigma_p$  is the standard deviation of the mean value of the coverage at which a left–right crossing first appears. Plots of  $\sigma_p$  versus  $L$  are shown for the objects (A2), (B) and (C) on a log–log scale in figure 2. The slope of these lines corresponds to the exponent  $1/\nu = 0.75 \pm 0.01$ .

### 3.1. Effects of anisotropy

Results for jamming densities and percolation thresholds are obtained for various probabilities of deposition in the horizontal direction, i.e. for values of the order parameter  $p$  ranging from  $p = 0$  to  $p = 1$ . Dependence of the percolation threshold  $\theta_p$  on the order parameter  $p$  are presented in figure 3 for various sizes of the basic objects from table 1. It can be seen that the lowest values of  $\theta_p$  are obtained for the isotropic case ( $p = 1/3$ ). Percolation threshold increases with the degree of anisotropy, having the largest values for fully oriented objects in one direction ( $p = 1$ ). This property is most pronounced for  $k$ -mers (figure 3(a)). Percolation thresholds for various values of the order parameter  $p$  for objects (A1), (A3), (A10), (A12), and (A20) are given in table 3. On the other hand, for triangles (C), neither jamming nor percolation are affected by the anisotropy (figure

Percolation in irreversible deposition on a triangular lattice: effects of anisotropy

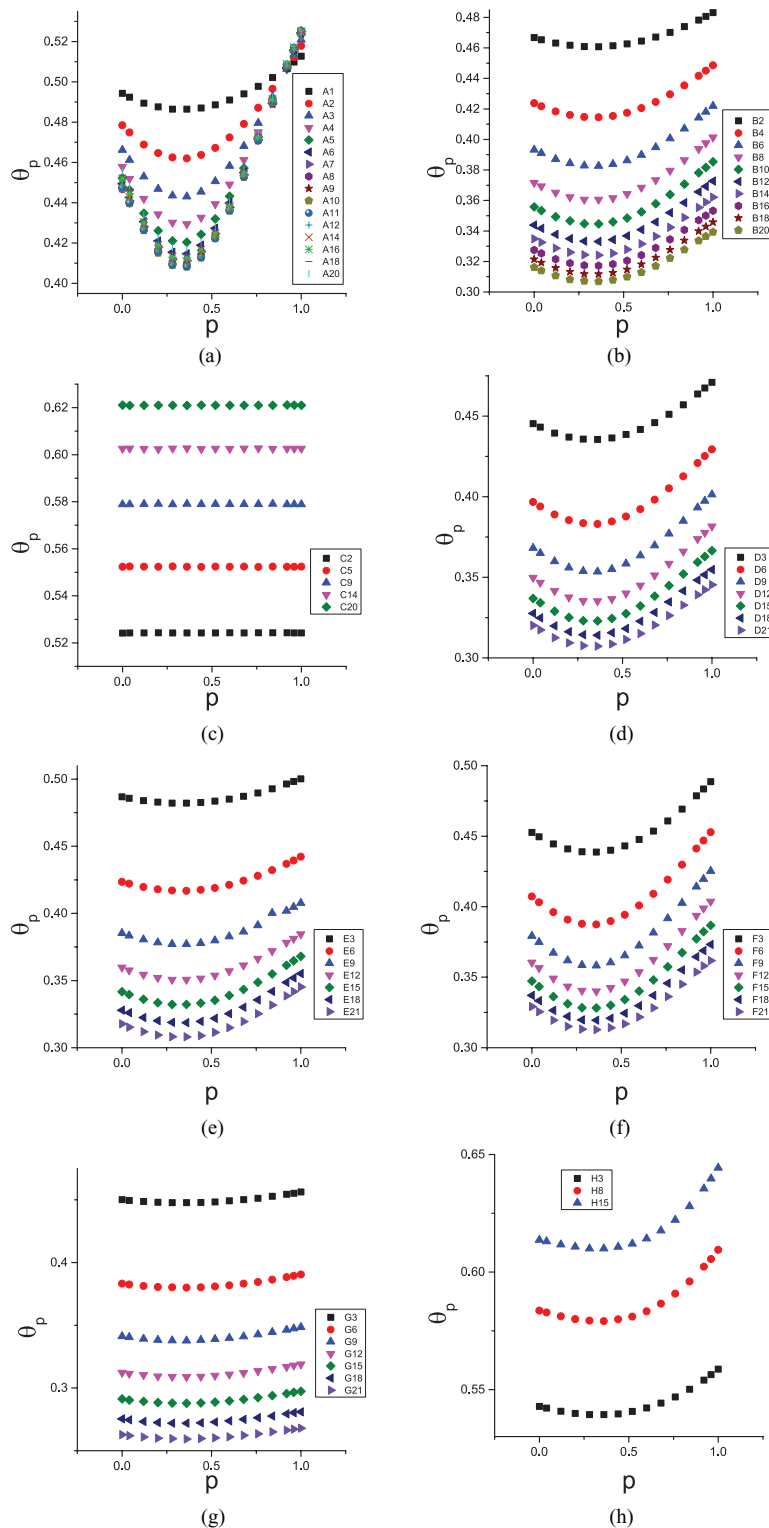


**Figure 3.** Dependence of the percolation threshold  $\theta_p$  on the probability  $p$  for deposition in the horizontal direction, i.e. on the order parameter, for various basic objects from table 1 and for the larger sizes of these shapes: (a) (A); (b) (B); (c) (C); (d) (D); (e) (E); (f) (F); (g) (G) and (h) (H).

**Table 3.** Percolation thresholds for various values of the order parameter  $p$  for objects (A1), (A3), (A10), (A12), and (A20).

| $p$  | $\theta_p$  |            |            |            |           |
|------|-------------|------------|------------|------------|-----------|
|      | A1          | A3         | A10        | A12        | A20       |
| 0    | 0.4943(12)  | 0.4662(14) | 0.4471(25) | 0.4482(27) | 0.456(4)  |
| 0.04 | 0.4924(11)  | 0.4612(14) | 0.4398(25) | 0.4410(26) | 0.448(3)  |
| 0.12 | 0.4894(11)  | 0.4530(12) | 0.4262(23) | 0.4271(26) | 0.434(3)  |
| 0.20 | 0.4876(11)  | 0.4469(14) | 0.4151(23) | 0.4160(26) | 0.423(3)  |
| 0.28 | 0.4864(12)  | 0.4436(13) | 0.4091(23) | 0.4097(25) | 0.418(3)  |
| 0.36 | 0.4864(10)  | 0.4430(12) | 0.4082(21) | 0.4090(23) | 0.417(3)  |
| 0.44 | 0.4870(11)  | 0.4455(13) | 0.4127(23) | 0.4133(24) | 0.421(3)  |
| 0.52 | 0.4886(11)  | 0.4507(13) | 0.4224(22) | 0.4225(27) | 0.428(3)  |
| 0.60 | 0.4910(11)  | 0.4583(13) | 0.4360(23) | 0.4364(27) | 0.440(4)  |
| 0.68 | 0.4940(11)  | 0.4681(14) | 0.4529(24) | 0.4534(28) | 0.457(4)  |
| 0.76 | 0.4977(11)  | 0.4795(12) | 0.4713(26) | 0.4718(28) | 0.475(4)  |
| 0.84 | 0.5021(11)  | 0.4904(16) | 0.4899(24) | 0.4905(26) | 0.494(4)  |
| 0.92 | 0.5073(11)  | 0.5064(15) | 0.5079(27) | 0.5084(29) | 0.5094(4) |
| 0.96 | 0.50984(11) | 0.5134(16) | 0.5169(25) | 0.5169(29) | 0.516(4)  |
| 1    | 0.5127(11)  | 0.5209(15) | 0.5255(26) | 0.5252(29) | 0.524(4)  |

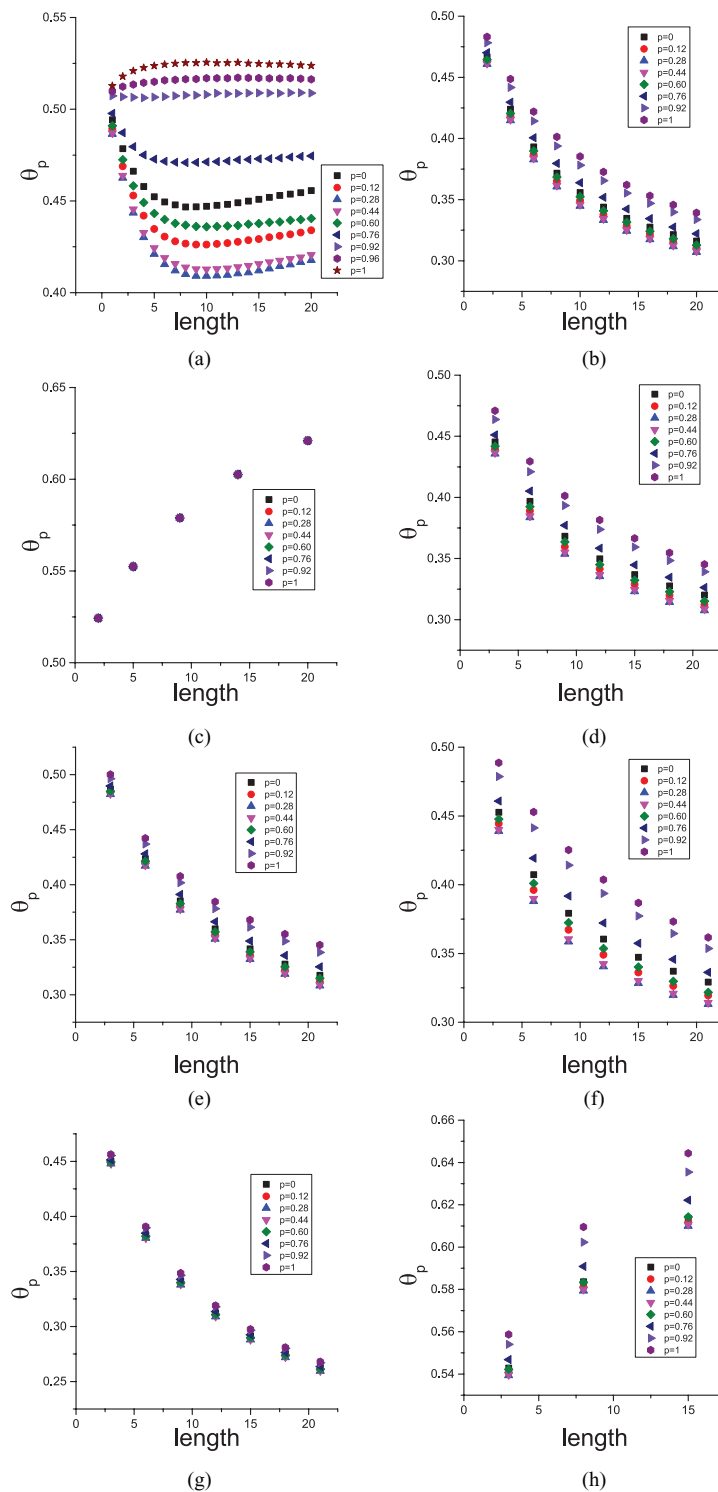
3(c)). The relative increase of the percolation threshold due to the complete alinement (maximum anisotropy) defined as:

$$R = \frac{\theta_p(p=1) - \theta_p(p=1/3)}{\theta_p(p=1/3)}, \quad (4)$$

is largest for the  $k$ -mers of length  $\ell = 11$  (A11), and its value is 28.6%. The lowest effect of the anisotropy (the lowest value of  $R$ ) on the studied  $k$ -mers is found for dimers: (4.8%). It is interesting that the percolation thresholds for  $k$ -mers of various lengths have almost the same values for highly anisotropic deposition. The minimum and maximum relative increase of the percolation threshold for  $p = 1$ , compared to the isotropic case, is given in table 4 for all objects from table 1. It can be seen that the impact of anisotropy on the percolation properties is largest for the elongated objects ((A), (F)), on the contrary to the compact rhombuses (H), that are less affected by the anisotropic conditions. With the exception of fully symmetrical objects, the increase in the anisotropy always results in higher percolation thresholds. It should be emphasized that the statistical errors are typically of the order of  $10^{-3}$ , and in all the figures the error bars are smaller than the symbol size.









It is interesting to note that there has been an uncertainty whether percolation can be reached for unlimited lengths of  $k$ -mers. Numerical investigations of this point would require extremely large lattices and the conclusions would still be based on extrapolation of the results obtained for relatively short  $k$ -mers. The solution of this dilemma can be found in [36], where the authors provided a rigorous proof that all jamming configurations of  $k$ -mers on a square lattice are percolating ones. In the isotropic case, percolation threshold decreases with  $\ell$  for shorter  $k$ -mers, reaches a smooth minimum for  $\ell \simeq 11$ , and slightly increases for longer  $k$ -mers [24]. Dependence of the percolation threshold on the length of various objects from table 1 is shown in figure 4 for some values of the order parameter  $p$ . Introducing the anisotropy shifts the minimum towards lower  $k$ -mer lengths. For highly anisotropic conditions a qualitatively different behavior

Percolation in irreversible deposition on a triangular lattice: effects of anisotropy



**Figure 4.** Dependence of the percolation threshold  $\theta_p$  on the length of various objects from table 1: (a) (A); (b) (B); (c) (C); (d) (D); (e) (E); (f) (F); (g) (G) and (h) (H) for the values of the order parameter:  $p = 0; 0.12; 0.28; 0.44; 0.60; 0.76; 0.92$  and 1.

**Table 4.** Relative increase of the percolation threshold (equation (4)) for  $p = 1$ , comparing to the fully isotropic case.

| ( $x$ ) | Shape                                                                             | $R_{\min.}-R_{\max.}$ | Objects                   |
|---------|-----------------------------------------------------------------------------------|-----------------------|---------------------------|
| (A)     |  | 4.8%–28.6%            | $A1$ (min.); $A11$ (max.) |
| (B)     |  | 4.8%–8.2%             | $B2$ (min.); $B14$ (max.) |
| (C)     |  | /                     | /                         |
| (D)     |  | 8.1%–13.4%            | $D3$ (min.); $D9$ (max.)  |
| (E)     |  | 3.7%–12.1%            | $E3$ (min.); $E21$ (max.) |
| (F)     |  | 11.4%–18.8%           | $F3$ (min.); $F9$ (max.)  |
| (G)     |  | 3.7%–12.1%            | $G3$ (min.); $G21$ (max.) |
| (H)     |  | 3.6%–5.6%             | $H3$ (min.); $H15$ (max.) |

**Table 5.** Percolation thresholds for various lengths of  $k$ -mers for  $p = 0$ ,  $p = 0.12$ ,  $p = 1/3$ ,  $p = 0.76$ ,  $p = 0.92$ , and  $p = 1$ .

| Length | $\theta_p$ |            |            |            |            |            |
|--------|------------|------------|------------|------------|------------|------------|
|        | $p = 0$    | $p = 0.12$ | $p = 1/3$  | $p = 0.76$ | $p = 0.92$ | $p = 1$    |
| 1      | 0.4943(12) | 0.4894(11) | 0.4863(11) | 0.4977(11) | 0.5073(11) | 0.5127(11) |
| 2      | 0.4785(13) | 0.4689(12) | 0.4620(11) | 0.4872(12) | 0.5067(13) | 0.5179(13) |
| 3      | 0.4662(14) | 0.4530(12) | 0.4428(13) | 0.4795(15) | 0.5064(15) | 0.5209(15) |
| 4      | 0.4578(16) | 0.4420(16) | 0.4293(15) | 0.4751(16) | 0.5062(16) | 0.5225(17) |
| 5      | 0.4523(18) | 0.4348(17) | 0.4202(16) | 0.4728(18) | 0.5066(18) | 0.5236(19) |
| 6      | 0.4494(20) | 0.4306(18) | 0.4145(17) | 0.4716(19) | 0.5068(20) | 0.5243(20) |
| 7      | 0.4479(20) | 0.4281(20) | 0.4110(18) | 0.4711(21) | 0.5161(21) | 0.5249(22) |
| 8      | 0.4468(23) | 0.4268(20) | 0.4088(21) | 0.4708(22) | 0.5076(22) | 0.5252(25) |
| 9      | 0.4468(24) | 0.4263(22) | 0.4079(21) | 0.4710(24) | 0.5076(27) | 0.5252(23) |
| 10     | 0.4471(25) | 0.4263(23) | 0.4078(22) | 0.4713(26) | 0.5079(27) | 0.5255(26) |
| 11     | 0.4476(27) | 0.4266(24) | 0.4080(23) | 0.4714(26) | 0.5087(26) | 0.5251(29) |
| 12     | 0.4482(27) | 0.4271(26) | 0.4087(24) | 0.4718(28) | 0.5084(29) | 0.5252(29) |
| 13     | 0.4490(27) | 0.4278(29) | 0.4095(26) | 0.472(3)   | 0.509(3)   | 0.5253(29) |
| 14     | 0.450(3)   | 0.4287(29) | 0.4104(25) | 0.473(4)   | 0.509(3)   | 0.525(3)   |
| 15     | 0.451(3)   | 0.429(3)   | 0.4112(27) | 0.473(3)   | 0.509(3)   | 0.525(3)   |
| 16     | 0.452(3)   | 0.430(3)   | 0.4124(29) | 0.473(4)   | 0.509(4)   | 0.525(4)   |
| 17     | 0.453(3)   | 0.431(3)   | 0.4134(29) | 0.473(4)   | 0.509(4)   | 0.524(3)   |
| 18     | 0.454(3)   | 0.432(3)   | 0.415(3)   | 0.474(4)   | 0.509(4)   | 0.524(4)   |
| 19     | 0.454(3)   | 0.433(3)   | 0.415(3)   | 0.474(4)   | 0.509(4)   | 0.524(4)   |
| 20     | 0.456(4)   | 0.434(3)   | 0.417(3)   | 0.475(4)   | 0.509(4)   | 0.524(4)   |

is obtained— $\theta_p$  increases with the  $k$ -mer length, reaches a maximum, and decreases for longer  $k$ -mers (figure 4(a)). Percolation thresholds for various lengths of  $k$ -mers for  $p = 0$ ,  $p = 0.12$ ,  $p = 1/3$ ,  $p = 0.76$ ,  $p = 0.92$ , and  $p = 1$  are given in table 5. For the angled objects (B)  $\theta_p$  decreases with  $\ell$  (figure 4(b)), but for the triangles (C) increases with the object size (figure 4(c)). Numerical values of the percolation thresholds for various lengths of angled objects (B) for  $p = 0$ ,  $p = 1/3$ ,  $p = 0.76$ , and  $p = 1$  are given in table 6. There is an essential difference between deposition of elongated objects and the compact ones. This feature is connected with difference in the geometry exclusion effects. Blocking of the substrate area is enhanced by the growth of the  $k$ -mer length, making the surface more porous. The porosity of the surface is also responsible for

**Table 6.** Percolation thresholds for various lengths of angled objects (B) for  $p = 0$ ,  $p = 1/3$ ,  $p = 0.76$ , and  $p = 1$ .

| Length | $\theta_p$ |            |            |            |
|--------|------------|------------|------------|------------|
|        | $p = 0$    | $p = 1/3$  | $p = 0.76$ | $p = 1$    |
| 2      | 0.4667(11) | 0.4608(12) | 0.4701(11) | 0.4831(11) |
| 4      | 0.4239(14) | 0.4146(12) | 0.4296(12) | 0.4487(12) |
| 6      | 0.3932(14) | 0.3825(13) | 0.4006(13) | 0.4219(13) |
| 8      | 0.3716(16) | 0.3602(14) | 0.3796(15) | 0.4014(14) |
| 10     | 0.3558(15) | 0.3445(16) | 0.3638(15) | 0.3853(16) |
| 12     | 0.3439(17) | 0.3329(17) | 0.3519(17) | 0.3727(16) |
| 14     | 0.3348(19) | 0.3239(19) | 0.3423(19) | 0.3621(21) |
| 16     | 0.3275(20) | 0.3171(20) | 0.3345(18) | 0.3532(18) |
| 18     | 0.3214(23) | 0.3116(21) | 0.3276(20) | 0.3458(18) |
| 20     | 0.3161(22) | 0.3071(22) | 0.3221(19) | 0.3393(19) |

the decrease of  $\theta_p$  with the length of the angled objects (B), as well as for the objects (D), (E), (F) and (G) from table 1. On the other hand, for compact objects, such as triangles (C) and rhombuses (H), percolation threshold increases with their size. This is the consequence of a low connectivity of these objects.

Figure 5 shows the ratio  $\theta_p/\theta_{\text{jam}}$  versus the order parameter  $p$  for various sizes of the objects from table 1. These plots also exhibit a minimum for the isotropic case and grow with the order parameter  $p$ . For larger sizes of elongated shapes such as (A), (B), (D), (F), this minimum is more prominent. Less elongated shapes (E), (G), (H) show a broad minimum for the isotropic case, and an abrupt increase of  $\theta_p/\theta_{\text{jam}}$  when  $p$  tends to unity. For such objects the  $\theta_p/\theta_{\text{jam}}$  ratio is only slightly affected by the low degree of anisotropy, but increases significantly when depositing conditions impose almost complete alignment of the objects.

Percolation threshold behavior for various objects from table 1 is illustrated in figure 6 for a relatively high degree of the anisotropy  $p = 0.84$ . Under these conditions,  $k$ -mer percolation practically does not depend on their length. For compact objects, triangles (C) and rhombuses (H), percolation threshold increases with  $\ell$ , while for the objects (B), (D), (E), (F) and (G) decreases with the object length. Jamming coverage decreases with the object size for all shapes of depositing objects [35]. When the dependence of the ratio  $\theta_p/\theta_{\text{jam}}$  on the object size is presented for various object shapes as in figure 7, it can be concluded that  $\theta_p/\theta_{\text{jam}}$  monotonically increases with  $\ell$  for each object shape. Namely, at very early times of the deposition process, depositing objects do not ‘feel’ the presence of already deposited ones, and are placed randomly according to the deposition rules onto the lattice. With the growth of the coverage, parallel deposition of elongated objects is more favored in order to avoid an intersection. Anisotropic conditions, i.e. ordering along one of the directions, show an additional deposition-induced alignment of the elongated objects. Percolation threshold for these objects decreases more slowly with  $\ell$  than the corresponding jamming coverage. This results in the increase of the  $\theta_p/\theta_{\text{jam}}$  ratio. On the other hand, anisotropic deposition of compact objects, triangles (C) and rhombuses (H), gives the increase of the percolation threshold with the object size, resulting in the increase of  $\theta_p/\theta_{\text{jam}}$  with  $\ell$ .

Percolation in irreversible deposition on a triangular lattice: effects of anisotropy

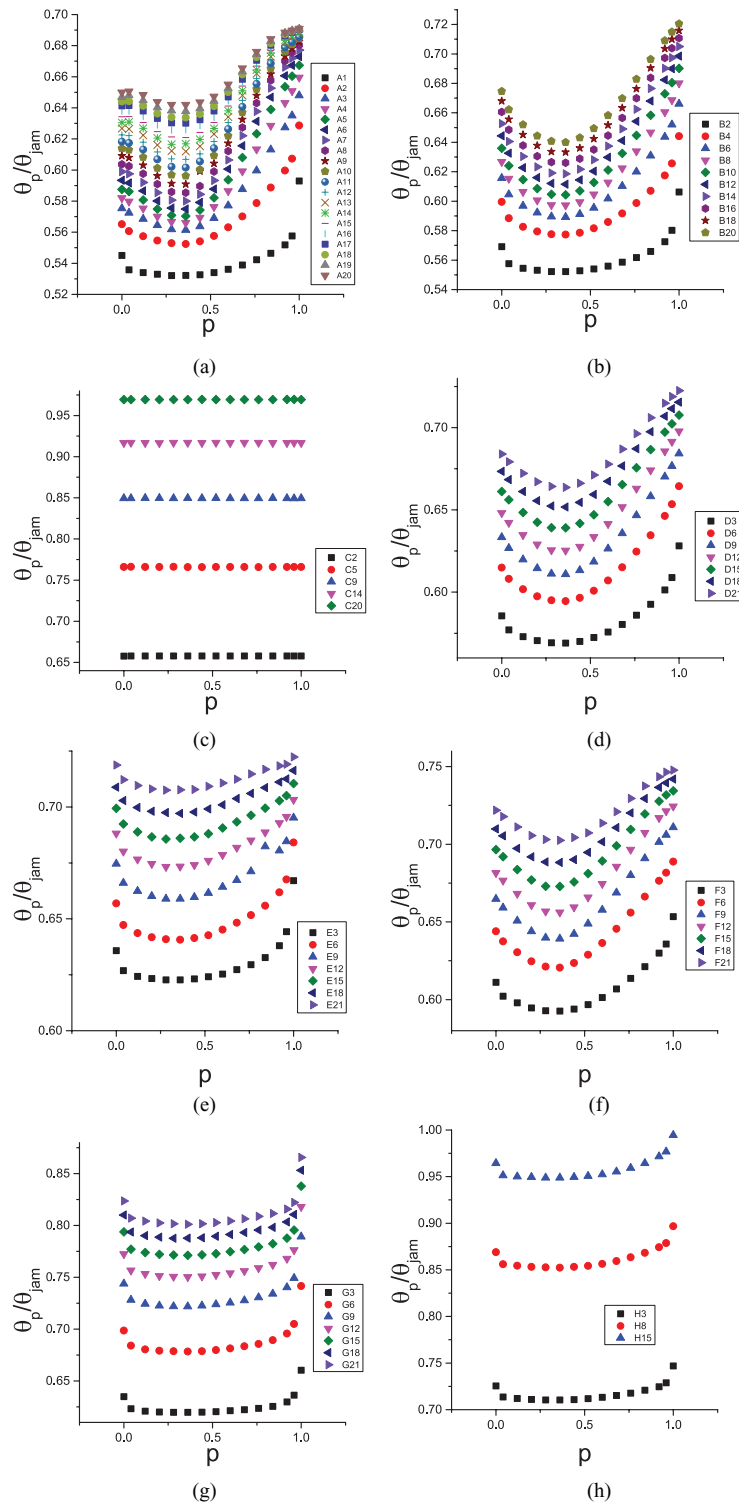


**Figure 5.** Dependence of  $\theta_p/\theta_{jam}$  on the probability  $p$  for deposition in the horizontal direction, i.e. on the order parameter, for various objects from table 1 and for the larger sizes of these shapes: (a) (A); (b) (B); (c) (C); (d) (D); (e) (E); (f) (F); (g) (G) and (h) (H).

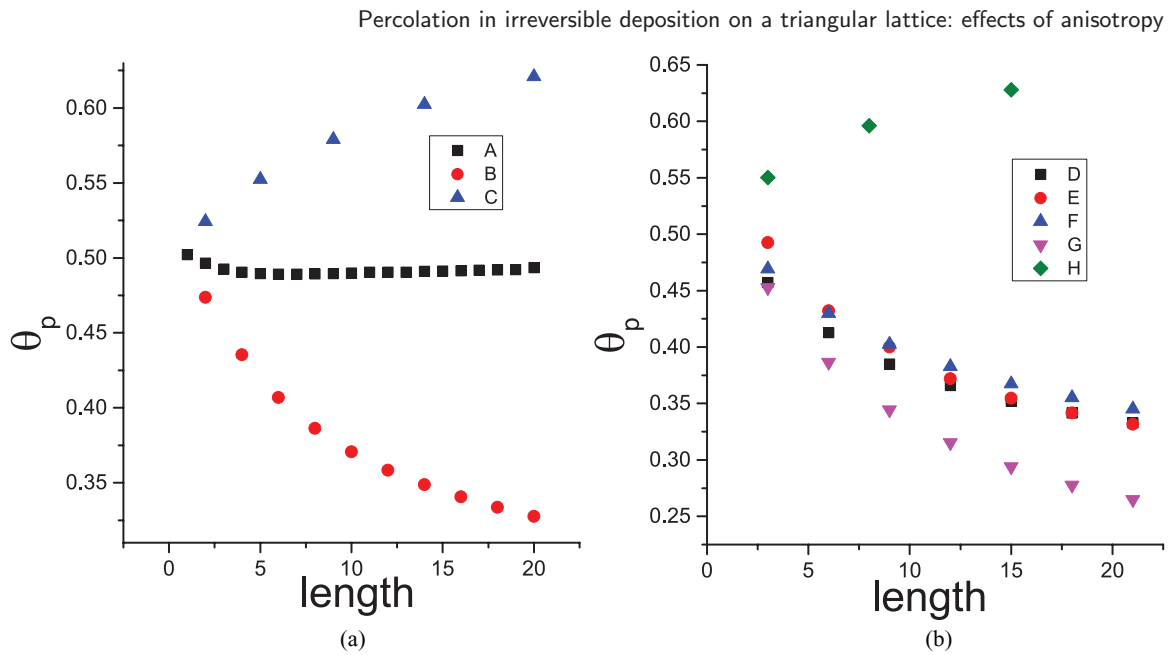


**Figure 6.** (a) Dependence of the percolation threshold  $\theta_p$  on the length of objects (A), (B), and (C) from table 1 for  $p = 0.84$ . (b) Dependence of the percolation threshold  $\theta_p$  on the length of objects (D), (E), (F), (G), and (H) from table 1 for  $p = 0.84$ .

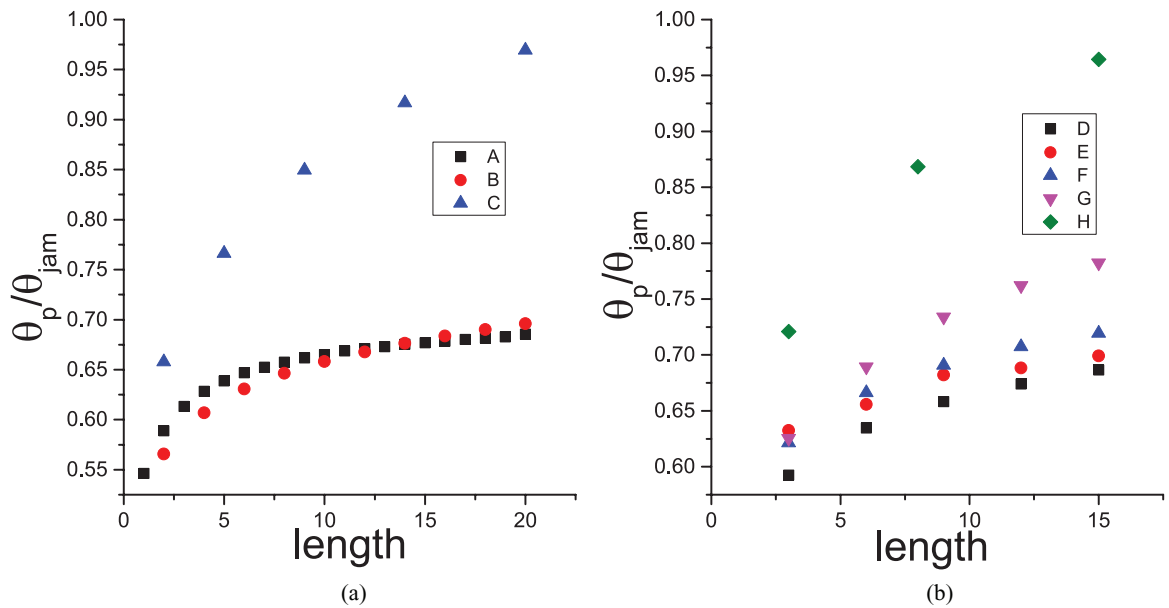


**Figure 7.** (a) Dependence of  $\theta_p/\theta_{jam}$  on the length of objects (A), (B), and (C) from table 1 for  $p = 0.84$ . (b) Dependence of  $\theta_p/\theta_{jam}$  on the length of objects (D), (E), (F), (G), and (H) from table 1 for  $p = 0.84$ .

Comparison of the fully aligned adsorption ( $p = 1$ ) and the isotropic case is illustrated in figure 8. Dependence of the percolation threshold on the length of objects (A), (B) and (C) from table 1 are shown for  $p = 1$  and for the isotropic case ( $p = 1/3$ ). Existence of the anisotropy in the adsorption process results in the increase of the percolation threshold. The most noticeable effect is for the adsorption of line-segments

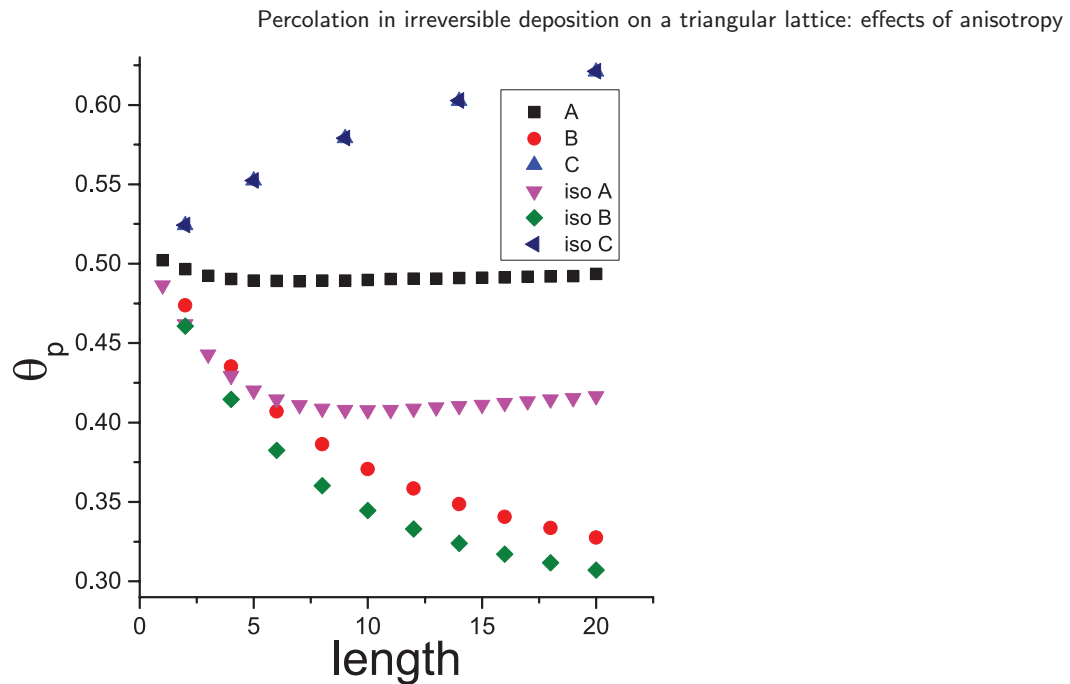


**Figure 8.** Dependence of the percolation threshold  $\theta_p$  on the length of objects (A), (B) and (C) from table 1 for  $p = 1$  and for the isotropic case ( $p = 1/3$ ), as indicated in the legend.

( $k$ -mers), for which the percolation threshold in the isotropic case decreases with  $\ell$ , reaches a minimum, and increases for longer  $k$ -mers, while for the fully aligned deposition,  $\theta_p$  increases with  $\ell$  for short  $k$ -mers, reaches a maximum, and slightly decreases for longer objects. As already mentioned, deposition properties of triangles with the symmetry axis of third order, are not affected by the presence of anisotropy. The same conclusion would apply to the adsorption of hexagons with symmetry axis of sixth order, matching the underlying triangular lattice.

### 3.2. Percolation in anisotropic conditions on a lattice with point-like defects

Percolation properties are also examined for inhomogeneous substrates, with quenched impurities and anisotropic depositing conditions. The aim of these numerical experiments is to examine how the defects, together with the anisotropic depositing conditions, affect the percolating properties of the deposits.

In the work [31] percolation thresholds were determined for  $k$ -mers, angled objects, and triangles of two different sizes. It was found that for the examined  $k$ -mers,  $\theta_p$  was practically not affected by the presence of point-like impurities. For the deposition of triangles, a slight decrease of  $\theta_p$  was observed with the increase of the point-like defect concentration.

Simulations of the irreversible deposition on a substrate containing defects are performed in two steps. The triangular lattice is initially and randomly occupied by point-like defects at given concentration  $d$ . After placing the impurities, anisotropic deposition of objects of various shapes is performed. The depositing objects are not allowed to overlap with the previously deposited ones, nor with the lattice defects.

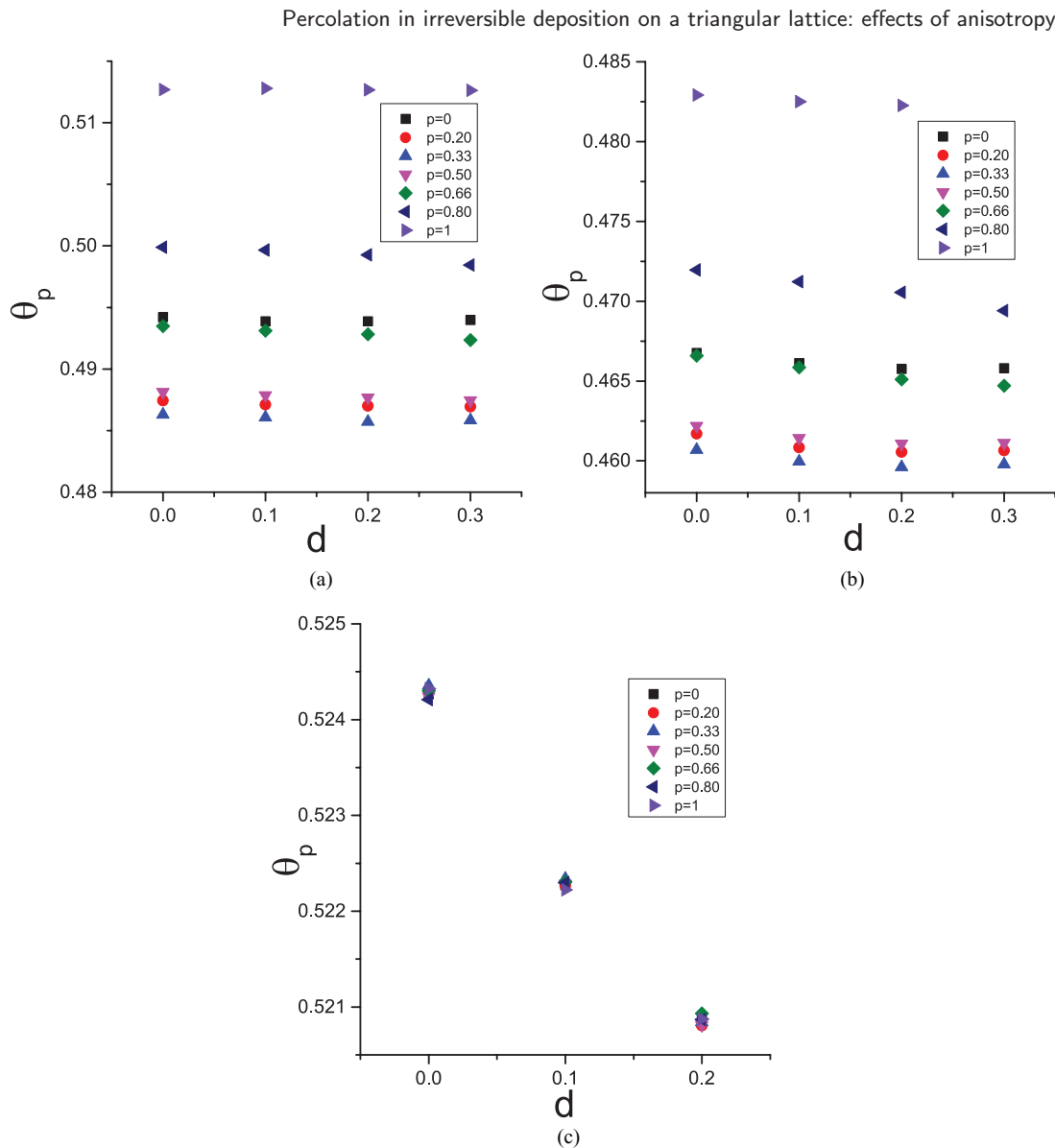


**Figure 9.** Dependence of the percolation threshold  $\theta_p$  on the impurity concentration  $d$  for various values of the order parameter  $p$  for objects: (a) (A2), (b) (B), and (c) (C).

Results are obtained for various degrees of anisotropy determined by the values of the order parameter  $p = 0; 0.20; 0.33; 0.50; 0.66; 0.80$  and  $1$ . Plots of the percolation threshold  $\theta_p$  versus the defect concentration  $d$  are shown in figure 9 for line segments covering three lattice sites (A2), angled objects (B) and triangles (C) from table 1. From figure 9(a) we can see that the percolation threshold for the  $k$ -mers covering three lattice sites is almost not affected by the impurity concentration  $d$ . Formation of a percolation cluster requires a certain coverage by the depositing  $k$ -mers, and this is not changed by the presence of the point-like impurities that are avoided by the depositing line-segments. The situation is similar for the angled objects (B), although the values of the percolation thresholds are lower than for the line segments. A slight decrease of the percolation threshold with the impurity concentration can be observed. However,

for both of these shapes,  $\theta_p$  significantly increases with the degree of anisotropy. The lowest values of  $\theta_p$  are obtained for the fully isotropic case ( $p = 0.33$ ), and the highest for the completely aligned objects ( $p = 1$ ). Plots of  $\theta_p$  versus the defect concentration  $d$  for the triangles ( $C$ ) are qualitatively different. The percolation threshold decreases with  $d$ , but is not affected by the presence of anisotropy.

#### 4. Concluding remarks

Percolation properties in anisotropic irreversible deposition on inhomogeneous substrates have been investigated. Various object shapes were examined and percolation thresholds were determined for various degrees of deposition anisotropy characterized by the order parameter  $p$  = taking values from  $p = 0$  to  $p = 1$ . It was found that the percolation threshold increases with the degree of anisotropy, having the maximum values for fully oriented objects in one direction. The relative increase of the percolation threshold for the maximum anisotropy ( $p = 1$ ), compared to the isotropic case ( $p = 1/3$ ), is largest for  $k$ -mers of length  $\ell = 11$ . These are the  $k$ -mers that give the lowest value of  $\theta_p$  in the isotropic case. On the contrary, percolation of the triangles with the symmetry axis of third order, is not affected by the anisotropy of the underlying lattice.

Essential difference in the percolation properties of elongated and compact objects was also found. High porosity of the deposit and the high connectivity of elongated objects result in low percolation thresholds for the isotropic, as well as for the anisotropic deposition. For these objects  $\theta_p$  decreases with their size. On the other hand, low connectivity of the compact objects, for example triangles and rhombuses, results in higher percolation thresholds, while  $\theta_p$  increases with the object size. It should be noted that the  $k$ -mers show a more complex behavior. For the isotropic case  $\theta_p$  decreases with  $\ell$  for shorter  $k$ -mers, reaches a minimum, and increases for longer  $k$ -mers. In the presence of anisotropy the minimum is shifted towards shorter  $k$ -mers. For highly anisotropic deposition, percolation threshold practically does not depend on the  $k$ -mer length.

Simulations of adsorption processes on anisotropic substrates with defects showed a qualitatively different behavior of the percolation threshold for different object shapes. In the case of  $k$ -mer deposition, percolation threshold is not affected by the presence of point-like impurities, for angled objects  $\theta_p$  slightly decreases with the impurity concentration, and this decrease is most prominent for compact objects (triangles). Percolation threshold increases with the degree of anisotropy, with the exception of triangle deposition that is not affected by the presence of anisotropy.

#### Acknowledgments

This work was supported by the Ministry of Education, Science, and Technological Development of the Republic of Serbia under projects ON171017, III45016, and by the European Commission under H2020 project VI-SEEM, Grant No. 675121. Numerical simulations were run on the PARADOX supercomputing facility at the Scientific Computing Laboratory of the Institute of Physics Belgrade.

## References

- [1] Ciesla M 2013 Continuum random sequential adsorption of polymer on a flat and homogeneous surface *Phys. Rev. E* **87** 052401
- [2] Dabrowski A 2001 Adsorption from theory to practice *Adv. Colloidal Interface Sci.* **93** 135–224
- [3] Rabe M, Verdes D and Seeger S 2011 Understanding protein adsorption phenomena at solid surfaces *Adv. Colloid Interface Sci.* **162** 87–106
- [4] Cadilhe A, Araujo N A M and Privman V 2007 Random sequential adsorption: from continuum to lattice and pre-patterned substrates *J. Phys.: Condens. Matter* **19** 065124
- [5] Tsukruk V V, Ko H and Palashenko S 2004 Nanotube surface arrays: weaving, bending, and assembling on patterned silicon *Phys. Rev. Lett.* **92** 065502
- [6] Shim B S and Kotov N A 2005 Single-walled carbon nanotube combining during layer-by-layer assembly: from random adsorption to aligned composites *Langmuir* **21** 9381
- [7] Park C, Wilkinson J, Banda S, Ounaies Z, Wise K E, Sauti G, Lillehei P T and Harrison J S 2006 Aligned single-wall carbon nanotube polymer composites using an electric field *J. Polym. Sci. B* **44** 1751
- [8] Evans J W 1993 Random and cooperative sequential adsorption *Rev. Mod. Phys.* **65** 1281–329
- [9] Talbot J, Tajrus G, Van Tassel P R and Viot P 2000 From car parking to protein adsorption: an overview of sequential adsorption process *Colloids Surf. A* **165** 287–324
- [10] Privman V 2000 Dynamics of nonequilibrium deposition *Colloids Surf. A* **165** 231–40
- [11] Bartelt M C and Privman V 1991 Kinetics of irreversible adsorption of mixtures of pointlike and fixed-size particles: exact results *Phys. Rev. A* **44** R2227–30
- [12] Ben-Naim E and Krapivsky P L 1994 On irreversible deposition on disordered substrates *J. Phys. A: Math. Gen.* **27** 3575–7
- [13] Cornette V, Linares D, Ramirez-Pastor A J and Nieto F 2007 Random sequential adsorption of polyatomic species *J. Phys. A: Math. Theor.* **40** 11765–76
- [14] Ciesla M and Jakub Barbasz 2014 Random packing of regular polygons and star polygons on a flat two-dimensional surface *Phys. Rev. E* **90** 022402
- [15] Budinski-Petković L, Vrhovac S B and Lončarević I 2008 Random sequential adsorption of polydisperse mixtures on discrete substrates *Phys. Rev. E* **78** 061603
- [16] Ciesla M, Pajak G and Ziff R M 2016 In a search for a shape maximizing packing fraction for two-dimensional random sequential adsorption *J. Chem. Phys.* **145** 044708
- [17] Budinski-Petković L, Lončarević I, Dujak D, Karač A, Šćepanović J R, Jakšić Z M and Vrhovac S B 2017 Particle morphology effects in random sequential adsorption *Phys. Rev. E* **95** 022114
- [18] Garcia G D, Sanchez-Varretti F O, Centres P M and Ramirez-Pastor A J 2015 Random sequential adsorption of straight rigid rods on a simple cubic lattice *Physica A* **436** 558–64
- [19] Stauffer D and Aharony A 1994 *Introduction to Percolation Theory* (London: Taylor and Francis)
- [20] Kondrat G and Pekalski A 2001 Percolation and jamming in random sequential adsorption of linear segments on a square lattice *Phys. Rev. E* **63** 051108
- [21] Rampf F and Albano E V 2002 Interplay between jamming and percolation upon random sequential adsorption of competing dimers and monomers *Phys. Rev. E* **66** 061106
- [22] Adamczyk P, Romiszowski P and Sikorski A 2008 A simple model of stiff and flexible polymer chain adsorption: the influence of internal chain architecture *J. Chem. Phys.* **128** 154911
- [23] Kondrat G 2008 Impact of composition of extended objects on percolation on a lattice *Phys. Rev. E* **78** 011101
- [24] Budinski-Petković Lj, Lončarević I, Petković M, Jakšić Z M and Vrhovac S B 2012 Percolation in random sequential adsorption of extended objects on a triangular lattice *Phys. Rev. E* **85** 061117
- [25] Lebovka N I, Karmazina N N, Tarasevich Y Y and Laptev V V 2011 Random sequential adsorption of partially oriented linear  $k$ -mers on a square lattice *Phys. Rev. E* **84** 061603
- [26] Budinski-Petković Lj, Lončarević I, Jakšić Z M, Vrhovac S B and Švrakić N M 2011 Simulation study of anisotropic random sequential adsorption of extended objects on a triangular lattice *Phys. Rev. E* **84** 051601
- [27] Du F, Fischer J E and Winey K I 2005 Effect of nanotube alignment on percolation conductivity in carbon nanotube/polymer composites *Phys. Rev. B* **72** 121404
- [28] Tarasevich Y Y, Goltseva V A, Laptev V V and Lebovka N I 2016 Electrical conductivity of a monolayer produced by random sequential adsorption of linear  $k$ -mers onto a square lattice *Phys. Rev. E* **94** 042112
- [29] Tarasevich Y Y, Lebovka N I and Laptev V V 2012 Percolation of linear  $k$ -mers on a square lattice: from isotropic through partially ordered to completely aligned sites *Phys. Rev. E* **86** 061116
- [30] Kondrat G 2005 The study of percolation with the presence of impurities *J. Chem. Phys.* **122** 184718

- [31] Lončarević I, Budinski-Petković Lj, Dujak D, Karać A, Jakšić Z and Vrhovac S B 2017 The study of percolation with the presence of extended impurities *J. Stat. Mech.* [093202](#)
- [32] Tarasevich Y Y, Burmistrov A S, Shinyaeva T S, Laptev V V, Vygornitskii N V and Lebovka N I 2015 Percolation and jamming of linear  $k$ -mers on a square lattice with defects: effect of anisotropy *Phys. Rev. E* **92** 062142
- [33] Newman M E J and Ziff R M 2001 Fast Monte Carlo algorithm for site or bond percolation *Phys. Rev. E* **64** 016706
- [34] Dujak D, Karać A, Budinski-Petković Lj, Lončarević I, Jakšić Z M and Vrhovac S B 2019 Percolation in random sequential adsorption of mixtures on a triangular lattice *J. Stat. Mech.* [113210](#)
- [35] Budinski-Petković Lj and Kozmidis-Luburić U 1997 Random sequential adsorption on a triangular lattice *Phys. Rev. E* **56** 6904
- [36] Kondrat G, Koza Z and Brzeski P 2017 Jammed systems of oriented needles always percolate on square lattices *Phys. Rev. E* **96** 022154